Effect of the Average Soft-Segment Length on the Morphology and Properties of Segmented Polyurethane Nanocomposites

Bradley Finnigan,[1] Peter Halley,[1] Kevin Jack,[2] Alasdair McDowell,[3] Rowan Truss,[1] Phil Casey,[4] Robert Knott,[5] Darren Martin[1]

[1]*School of Engineering, University of Queensland, Brisbane, Queensland 4072, Australia*
[2]*Centre for Nanotechnology and Biomaterials, University of Queensland, Brisbane, Queensland 4072, Australia*
[3]*Institute for Molecular Bioscience, University of Queensland, Brisbane, Queensland 4072, Australia*
[4]*Manufacturing and Infrastructure Technology, Commonwealth Scientific & Industrial Research Organization, Private Bag 33, Clayton South, VIC 3169, Australia*
[5]*Australian Nuclear Science and Technology Organisation, PMB 1, Menai, NSW 2234, Australia*

Received 4 September 2005; accepted 29 September 2005
DOI 10.1002/app.23347
Published online in Wiley InterScience (www.interscience.wiley.com).

ABSTRACT: Two organically modified layered silicates (with small and large diameters) were incorporated into three segmented polyurethanes with various degrees of microphase separation. Microphase separation increased with the molecular weight of the poly(hexamethylene oxide) soft segment. The molecular weight of the soft segment did not influence the amount of polyurethane intercalating the interlayer spacing. Small-angle neutron scattering and differential scanning calorimetry data indicated that the layered silicates did not affect the microphase morphology of any host polymer, regardless of the particle diameter. The stiffness enhancement on filler addition increased as the microphase separation of the polyurethane decreased, presumably because a greater number of urethane linkages were available to interact with the filler. For comparison, the small nanofiller was introduced into a polyurethane with a poly(tetramethylene oxide) soft segment, and a significant increase in the tensile strength and a sharper upturn in the stress–strain curve resulted. No such improvement occurred in the host polymers with poly(hexamethylene oxide) soft segments. It is proposed that the nanocomposite containing the more hydrophilic and mobile poly(tetramethylene oxide) soft segment is capable of greater secondary bonding between the polyurethane chains and the organosilicate surface, resulting in improved stress transfer to the filler and reduced molecular slippage. © 2006 Wiley Periodicals, Inc. J Appl Polym Sci 102: 128–139, 2006

Key words: morphology; nanoparticles; polyurethanes; structure-property relations

INTRODUCTION

Thermoplastic polyurethanes (TPUs) are linear, segmented copolymers consisting of alternating hard and soft segments. The hard segment is composed of alternating diisocyanate and short-chain-extender molecules (i.e., diol or diamine), whereas the soft segment is formed from a linear, long-chain diol. Phase separation occurs in TPUs because of the thermodynamic incompatibility of the hard and soft segments. The segments aggregate into microdomains, and this results in a structure consisting of glassy or semicrystalline hard domains and rubbery, soft domains, which are below and above their glass-transition temperatures (T_g's) at room temperature, respectively.

In recent times, nanometer-sized layered silicates have been introduced into many host polymers.[1–3] This interest was initiated by the large improvements in the stiffness and heat distortion temperature that Kojima et al.[4] achieved by incorporating layered silicates into nylon 6 at very low loadings (compared to traditional fillers). Experimental investigations have shown that layered silicates can significantly impact the microphase morphology of block copolymers and polymer blends by acting as templates for structure development.[5–8] Krishnamoorti and coworlers[6–8] studied the influence of the platelet size on the phase-separated morphologies of block copolymers[7,8] and polymer blends.[6] In these studies, Laponite (30 nm), montmorillonite (500 nm), and fluorohectorite (10 μm) were used to obtain the different size fractions. These studies revealed that the microphase morphologies of the block copolymers

Correspondence to: D. Martin (darrenm@cheque.uq.edu.au).
Contract grant sponsor: Australian Government Access to Major Facilities Program (through a travel grant to access the ISIS scattering facility).
Contract grant sponsor: University of Queensland Graduate School (through a travel grant to access the ISIS scattering facility).
Contract grant sponsor: University of Queensland (through a postgraduate research scholarship).

and polymer blends were dependent on the platelet size of the layered silicate.

Aside from the evidence that layered silicates can significantly change the microphase domain size and shape of block polymers and therefore lead to altered properties (and a potential route to controlling the morphology on the nanoscale), one would expect the size of the silicate particles to play an important role in the material properties in its own right. Wang and coworkers studied the effect of the silicate aspect ratio on the solid-state[9] and melt-state[10] properties of maleated polyethylene (ma-PE) nanocomposites and found that the composite containing the highest aspect ratio filler displayed superior properties and processability over the neat ma-PE and low-aspect-ratio filler composite.

Previous investigations into the effect of the layered silicate size on the nanocomposite structure and performance used different clay minerals to obtain the different size fractions.[6–11] Recently, we incorporated four different size fractions of Somasif MEE (organically treated, synthetic fluoromica; CBC Co., Ltd., Tokyo, Japan) into a segmented polyurethane.[12] This allowed us to investigate the effect of the particle size on the structure and properties of the host polymer without introducing additional variables (i.e., by not using different mineral types).

The smallest (S) and largest (L) size fractions of Somasif MEE from the previous study were used here. By varying the molecular weight of the polyurethane soft segment, we were able to study the influence of layered silicates on the structure and properties of TPUs with various degrees of microphase separation. For this purpose, three polymers were selected from a series of eight TPUs previously synthesized and characterized by Martin et al.[13,14] The chosen TPUs contained poly(hexamethylene oxide) (PHMO) soft segments, with molecular weights of 476, 793, and 998 g/mol, to provide morphologies ranging from phase-mixed (476 g/mol) to phase-separated (998 g/mol). All materials contained 60 wt % soft segment and 4,4′-methylene diphenyl diisocyanate (MDI) and 1,4-butanediol (BDO) hard segments. The results from this study are compared with those obtained in the previous investigation, in which MEE was incorporated into a TPU with a poly(tetramethylene oxide) (PTMO) soft segment and an MDI/BDO hard segment. Unlike the findings in other block copolymer nanocomposite systems, layered silicates did not affect the microphase morphology of the segmented polyurethanes studied here. The importance of the interaction between the soft segment and the organosilicate for achieving significant strength enhancements in these materials was identified, and the ability of the layered silicates to enhance the stiffness of the TPU was correlated to the degree of phase separation and urethane linkage concentration of the host polyurethane.

EXPERIMENTAL

Materials

Three TPUs consisting of PHMO soft segments with average molecular weights of 476, 793, and 998 g/mol and MDI and BDO hard segments were employed in this study. The TPUs are called 476, 793, and 998. The PHMO TPUs contained 40 wt % hard segment, and the synthesis of these materials has been described elsewhere.[13] The number-average molecular weights (M_n's) of 476, 793, and 998 were measured via gel permeation chromatography (GPC) to be 101,000, 53,000 and 63,000, respectively.

The PTMO TPU consisted of a 1000 g/mol PTMO soft segment and an MDI and BDO hard segment. The PTMO TPU contained 35 wt % hard segment and was supplied by Urethane Compounds (Melbourne, Australia). M_n was measured via GPC to be 216,000.

Somasif MEE was supplied by CO-OP Chemical Co. (Japan). MEE is a synthetic fluoromica with a chemical composition of $Na_{0.66}Mg_{2.68}(Si_{3.98}Al_{0.02})O_{10.02}F_{1.96}$ and a cation exchange capacity (CEC) of 115 mequiv/g.[15] The MEE variant of Somasif has a dipolyoxyethylenecocomethylammonium surface modification.[12]

Preparation

Different size fractions of MEE were obtained via a proprietary high-energy milling process. The preparation and characterization of these silicates have been described elsewhere.[12,16] The S and L size fractions were employed in this study. The inorganic fraction of both the small and large organosilicates was measured to be 78 wt % via thermogravimetric analysis. Size analysis via transmission electron microscopy (TEM)[17] indicated approximate effective diameters of 50–75 and 400–650 nm for the S and L organosilicates, respectively, in the PHMO host polymers. Nanocomposite films were prepared via solvent casting. A 5 wt % solution of dried MEE in toluene was ultrasonicated for 2 min before being added to a 5 wt % solution of TPU in dimethylacetamide. The combined solution was then mixed vigorously for 1 min in a high-shear homogenizer, and this was followed by stirring for 24 h at room temperature with a magnetic stirrer. The mixture was then cast onto glass plates, and the films were dried under a nitrogen atmosphere at 50°C for 48 h and subsequently dried *in vacuo* at 50°C for 12 h. The films were then annealed *in vacuo* at 80°C for 12 h and stored under ambient conditions for 1 month before characterization. The film thickness was 0.5 mm, and the composites contained 5 wt % organosilicate.

Characterization

TEM samples were cut on a Leica Ultracut S ultramicrotome (Wetzlar, Germany) with a Diatome diamond knife at −80°C and collected on 400-mesh copper grids. Images were obtained with a FEI Technai 12 TEM instrument (FEI Co., Eindhoven, The Netherlands) operated at 120 keV.

X-ray diffraction (XRD) analysis was carried out on a Bruker D8 Advance X-ray diffractometer (Bruker, Inc., Madison, WI, USA) with Cu Kα radiation generated at 40 kV and 30 mA. Samples were scanned at 2.4°/min in the range of 2θ = 1–0° with a step size of 0.02°. The MEE powders were lightly pressed and flattened to obtain a smooth surface before testing.

Thermogravimetric analysis of the organosilicates was carried out on a Shimadzu TGA 50 (Kyoto, Japan) under an air atmosphere. A heating rate of 10°C/min and a sample weight of approximately 10 mg were used.

Differential scanning calorimetry (DSC) measurements were performed on a TA Instruments 2920 MDSC instrument (New Castle, DE, USA). The sample weight was approximately 10 mg, and the heating rate was 10°C/min from −100 to 250°C.

Dynamic mechanical thermal analysis (DMTA) was performed on a Rheometric Scientific DMTA IV dynamic thermal mechanical analyzer (Piscataway, NJ, USA) equipped with a tensile head and reducing force option. The analysis was performed with a frequency of 2 Hz and a heating rate of 2°C/min from −120 to 100°C.

Tensile tests were carried out at 25°C on an Instron model 4505 universal testing machine (Norwood, MA, USA) with three replicates of each material. Dumbbells were punched from the films with an ASTM D 638-M-3 die and strained at 50 mm/min. Young's modulus was estimated from the slope at 0% strain on the tensile curve.

Small-angle neutron scattering (SANS) experiments were performed on the low Q (LOQ) station at the ISIS pulsed neutron source (Rutherford Appleton Laboratory, Oxfordshire, UK). The TPUs had sufficient neutron density contrast between the hard and soft phases such that deuteration was not required. A sample thickness of 1 mm and a beam diameter of 8 mm were used. Two-dimensional SANS data were collected over the course of 30 min for each sample. All neutron-scattering data were corrected for sample transmission, thickness, and background scattering. Thermal density fluctuations were corrected for the procedure of Bonart.[18] The data were converted to absolute units by calibration with a blend of deuterated and hydrogenated polystyrenes of known absolute cross sections.[19]

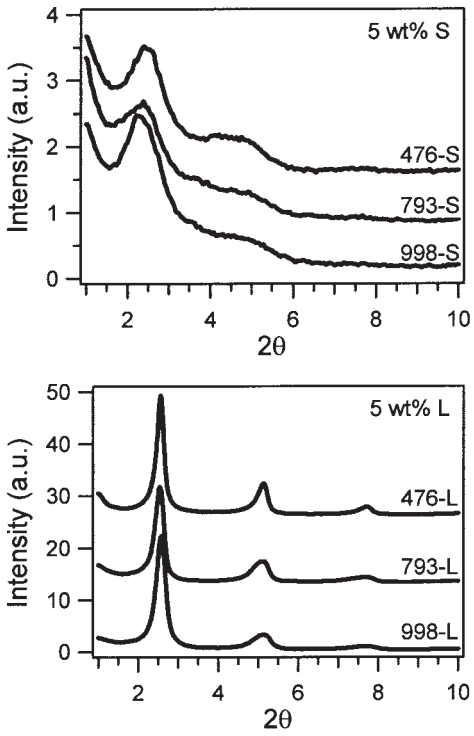

Figure 1 XRD patterns of the composites containing 5 wt % S and L organosilicates.

RESULTS AND DISCUSSION

XRD

XRD patterns of the composites containing 5 wt % S and L organosilicates are shown in Figure 1. The peak of highest intensity was assigned to the d_{001} reflection. The basal spacing was calculated from the position of this peak to be approximately 37 and 34.5 Å for the composites containing the S and L silicates, respectively. The basal spacings of the pristine S and L organosilicates were previously determined to be 22 and 21 Å, respectively.[12] This indicates that a significant amount of polyurethane was able to intercalate the interlayer spacing of both the S and L organosilicates. These results also suggest that the interlayer spacing of the organosilicates in the composites was not affected by the molecular weight of the PHMO soft segment within the range under investigation (476–998 g/mol). However, it would be an overinterpretation of the data to suggest that a greater amount of the polymer intercalated the interlayer spacing of the small silicates. A decrease in the stack size and ordering between layers causes a reduction in the magnitude of the structure factor term. Vaia and Liu[20] demonstrated that a weak structure factor, combined with the other angle-dependent terms that contribute to the scattering, results in the d_{001} peak being shifted to lower angles, and hence an apparent increase in the interlayer spacing is observed. The two silicates may

TABLE I
XRD Analysis

	Interlayer spacing (nm)	Average particle thickness (nm)	Average number of platelets/particle
476-S	3.7	16.4	4.4
793-S	3.7	16.4	4.4
998-S	3.7	12.9	3.3
476-L	3.45	79.0	22.9
793-L	3.45	64.4	18.7
998-L	3.45	59.9	17.3

therefore possess the same interlayer spacing despite the difference in the peak position shown in Figure 1.

The average stack size or particle thickness (L_Z) of the MEE particles in the composites was estimated with the Scherrer equation:

$$L_Z = 0.9\lambda / b \cos \theta \quad (1)$$

where λ is the X-ray wavelength, b is the full width at half-maximum of the d_{001} reflection, and θ is the scattering angle. The results are presented in Table I. The particle thickness calculated from the Scherrer equation is a lower bound estimate because internal disorder between the layers results in peak broadening.[20] In light of the previous discussion, the results presented for the composites containing the S organosilicate should be treated with particular caution because of their weak structural interference peaks. The particle thickness of the L organosilicate decreased from 79 to 60 nm as the molecular weight of the PHMO soft segment increased. This result suggests that the aspect ratio and degree of delamination of the L silicate improved as the soft-segment length increased. The extent to which platelets were peeled away from the particle stacks may have been influenced by the rheological characteristics of the nanocomposite solutions during the high shear mixing step of the processing route.

TEM

TEM images of the composites are shown in Figure 2 at magnifications of 18,500 and 97,000×. The mean effective diameters of the silicates in the three PHMO host polymers were estimated to be approximately 50–75 and 400–650 nm for the S and L size fractions, respectively. On the basis of the images available, the molecular weight of the PHMO soft segment did not appear to influence the dispersion or effective diameters of the layered silicates. The images did provide evidence suggesting that the S organosilicate dispersed less effectively in the PHMO TPUs than in the PTMO TPU previously investigated.[12] This might be a consequence of the higher hydrophobicity of the PHMO soft segment, which results from the additional methylene sequences per ether oxygen in the soft segment {i.e., HO—[$(CH_2)_n$—O—]$_m$H, where n is 4 and 6 for PTMO and PHMO, respectively}.

SANS

Laity et al.[21] assessed the ability of a number of scattering models based on different morphologies to reproduce the scattering features observed for segmented polyurethanes with various compositions. Spherical models based on a Zernike–Prins lattice or a Percus–Yevick liquid-type structure were found to most accurately fit the data. In light of this and our previous success in using these models to fit the scattering data from TPU nanocomposites subjected to uniaxial deformation,[12] these models were used here to analyze the SANS data.

Radially averaged one-dimensional (1D) SANS profiles of the three host polymers and the associated Percus–Yevick fits to the data are shown in Figure 3(a). The scattering peak observed for the 793 and 998 host polymers can be attributed to the periodicity in the microphase structure. The 476 host polymer was not modeled because it did not display a scattering peak. The absence of a scattering peak indicates a phase-mixed morphology. The increase in the intensity of the scattering peak with the molecular weight suggests that the extent of microphase separation increased with increasing segment length, and this is consistent with the findings of Martin et al.[13,14] This is because soft and hard-segment miscibility is reduced as the length of the soft and hard segments increase.[13]

The morphological data obtained from the Zernike–Prins and Percus–Yevick analyses are presented in Table II. The approximate volume fraction of hard segments participating in the hard domains (ϕ) was found to be 0.24 and 0.28 for the 793 and 998 host polymers, respectively. The TPUs employed in this study all contained 40 wt % hard segment. Assuming soft- and hard-segment densities of 1.04 and 1.32 g/cm^3, respectively,[22] ϕ would equal 0.344 if the TPUs were completely phase-separated. This result suggests that 70 and 80% hard segments are present in the hard domains of the 793 and 998 host polymers, respectively. Differences in the effective radius (R) and the standard deviation of the interdomain distance (σ) between the 793 and 998 host polymers were not significant within the estimated error range of the analysis. Commonly, a shell surrounding the spheres with the same scattering power as the surrounding matrix is assumed to exist.[21,23] The thickness of the shell (h) increases the minimum distance of the approach of the spheres. The average interdomain distance (d) was estimated to be 11 and 9 nm for the 793 and 998 polymers, respectively. The morphological data obtained from the Zernike–Prins and Percus–

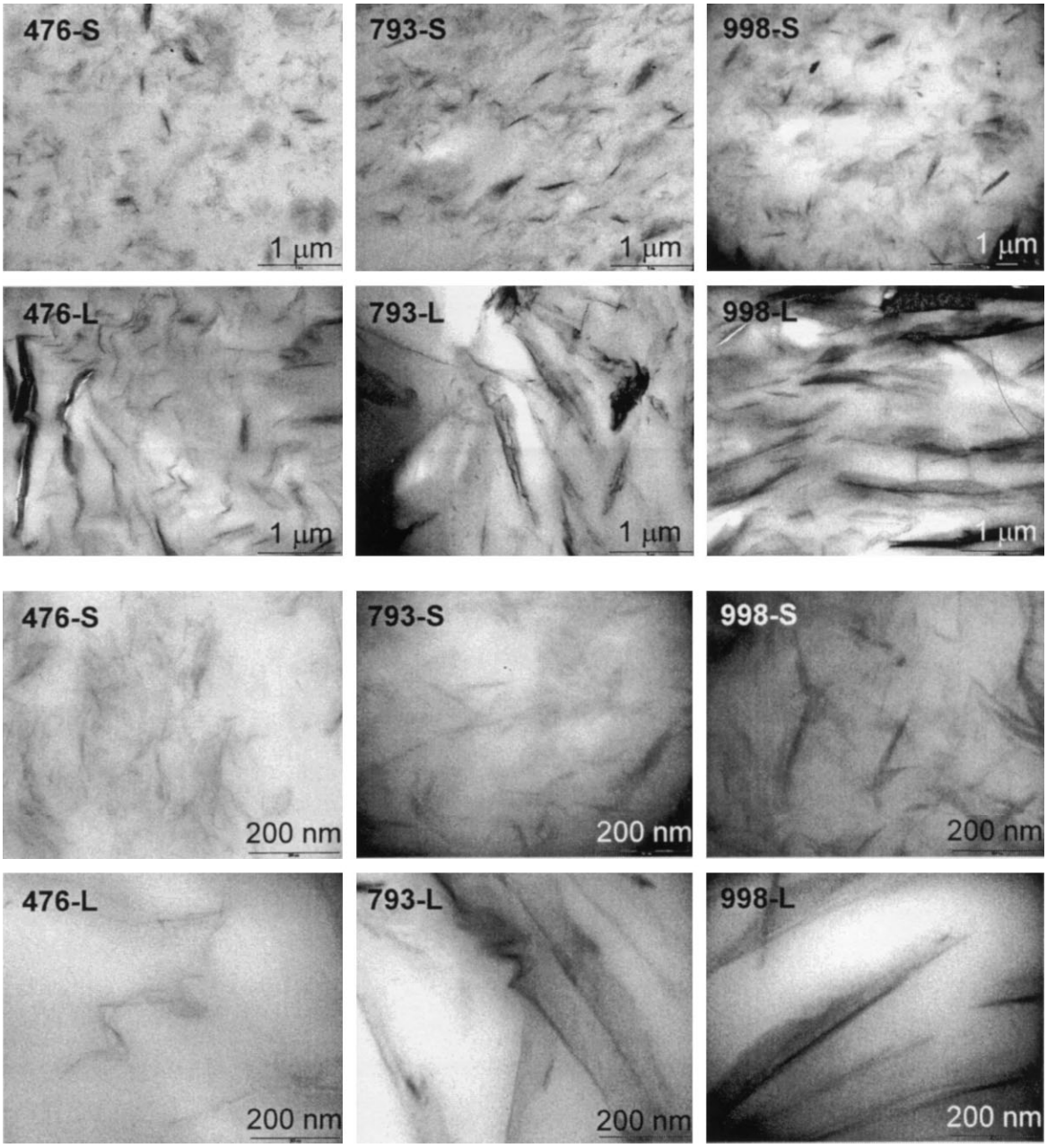

Figure 2 TEM images of the composites at magnifications of 18,500 and 97,000×.

Yevick analyses suggest that 998 had a microphase structure with a greater number of hard domains per unit of volume and a higher degree of phase separation than the 793 polymer.

Layered silicates exhibit a power-law dependence at q less than d_{001} or the interlayer spacing: $I(q) = Aq^m$, where I is the absolute scattering intensity, q is the scattering vector, A is a scaling factor consisting of both instrument and sample-dependent terms and m is a power law index that approaches $^{-}2$ for highly dispersed systems.[24] The scattering contribution from the silicates can be observed at low q as an upturn in intensity, and an example of this is shown for the 998 composites in Figure 3(b). At a 5 wt % loading, the MEE layered silicates did not have an effect on the scattering curves or the morphological data obtained from the Zernike–Prins and Percus–Yevick modeling. This suggests that the layered silicates did not alter the bulk microphase morphology of the 793 and 998 PHMO host polymers, regardless of the particle size. This is consistent with the findings for MEE dispersed in the PTMO TPU.[12]

The PHMO host polymers did not display the upturn in intensity at low q that was observed for the PTMO host polymer.[12] At present, the exact nature of the low q upturn is unknown, although it is most likely dependent

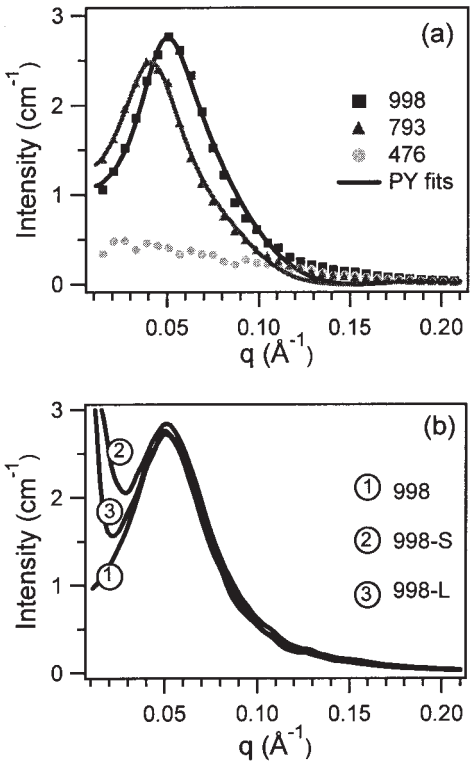

Figure 3 1D SANS profiles of (a) the host polymers and (b) 998 and its composites.

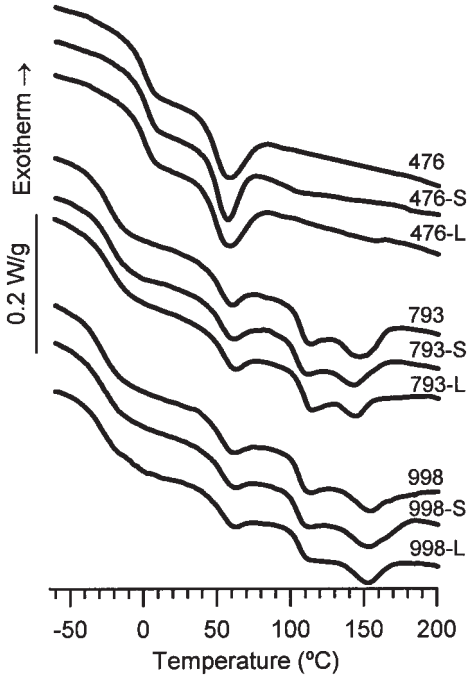

Figure 4 DSC thermograms.

on the nature of the interface between the soft and hard phases. Although it is possible to add a function to the hard sphere scattering model to account for the interface,[25] this was not attempted here.

DSC

DSC thermograms are shown in Figure 4, and a summary of the features is provided in Table III. An increase in the soft-segment molecular weight resulted in a decrease in the soft-phase T_g. This can be attributed to an increase in the purity of the soft phase and hence a reduction in the extent of molecular hindrance experienced by the soft segments in the vicinity of the hard segments.[13] Within the range of error, the heat capacity change (ΔC_p) associated with the glass transition was the same for all the materials. An increase in the molecular weight of the soft segment from 476 to 793 g/mol resulted in an increase in the temperature range over which the glass transition occurred (ΔT_g). Increasing the soft-segment molecular weight from 793 to 998 g/mol did not affect ΔT_g, nor did the addition of layered silicates to the host polymers. DMTA provides a more sensitive measure of T_g, and these results are discussed later.

TABLE II
Morphological Data Obtained from Zernike–Prins and Percus–Yevick Analyses of the SANS Data

	Zernike–Prins model			Percus–Yevick model		
	d (nm)	R (nm)	σ/d	ϕ	R (nm)	h (nm)
Uncertainty[a]	±0.5	±0.5	±0.05	±0.01	±0.5	±0.2
476	—	—	—	—	—	—
476-S	—	—	—	—	—	—
476-L	—	—	—	—	—	—
793	11.1	3.2	0.56	0.26	3.1	3.2
793-S	11.4	3.1	0.64	0.23	3.0	3.3
793-L	11.3	3.1	0.62	0.24	3.0	3.5
998	9.1	2.9	0.49	0.30	2.8	2.4
998-S	9.0	2.9	0.53	0.27	2.7	2.5
998-L	8.9	3.0	0.52	0.28	2.9	2.3

[a] Expected uncertainty due to sample variations and curve fitting.

TABLE III
Summary of the DSC Heating Curves

	Glass transition			Endotherms				
	T_g (°C)	ΔT_g (°C)	ΔC_p (J/g/°C)	T_1 (°C)		T_2 (°C)	ΔH_1 (J/g)	ΔH_2 (J/g)[a]
476	3	12	0.4	57	—		7.7 ± 1.4	—
476-S	3	12	0.4	60	—		6.8 ± 0.4	—
476-L	3	12	0.4	57	—		9.4 ± 1.1	—
793	−25	19	0.4	61	112	145	2.1 ± 1.1	29.5 ± 1.0
793-S	−25	19	0.4	60	112	144	3.1 ± 1.1	25.9 ± 1.5
793-L	−25	19	0.4	60	114	143	2.9 ± 0.3	24.4 ± 2.5
998	−28	19	0.4	59	114	153	3.1 ± 1.0	31.1 ± 4.9
998-S	−28	19	0.4	62	111	153	2.7 ± 0.2	29.9 ± 4.7
998-L	−29	19	0.4	62	111	152	2.1 ± 0.4	29.0 ± 4.8

[a] Enthalpies were calculated per gram of hard segment (not per gram of sample).
ΔH_1 and ΔH_2 correspond to melting enthalpies for the T_1 and bimodal T_2 endotherms.

In keeping with the nomenclature used in the previous investigations of these polymers, we labeled the endotherms observed in the DSC thermograms T_1 and T_2.[13,14] The addition of the layered silicates did not affect either the peak temperature or the enthalpy associated with the endotherms. The T_1, endotherm observed at approximately 60°C in Figure 4, was present in all the materials. This endotherm was assigned to the disordering of single MDI sequences and, in the case of 793 and 998, an additional contribution possibly caused by an enthalpy relaxation of hard segments at the hard-segment T_g. The enthalpy associated with the feature was approximately three times larger than that for the 476 material because of its high proportion of single MDI hard segments.[13,14]

A bimodal T_2 endotherm was observed for the 793 and 998 materials in the temperature range of 110–150°C. The first of the endotherms at 110°C, is the so-called annealing endotherm, which regularly occurs 20–50°C above the annealing temperature.[26–29] This endotherm has been ascribed to various phenomena, including a local restructuring of hard segments within the hard microdomains,[28,30,31] the disordering of hard-segment structures consisting predominantly of MDI–BDO–MDI hard segments,[13,14] an apparent hard microdomain glass-transition process,[32] hard-segment sequences that are capable of forming short-range ordered structures at the given annealing temperature[33] (where the hard-segment lengths participating in such structures are given by the Koberstein and Stein partial miscibility model),[34] and an enthalpy relaxation of the amorphous hard segment.[29]

The second endotherm (T_2) occurred at approximately 144 and 153°C for the 793 and 998 materials, respectively. Endotherms found in the temperature range of 140–200°C have been attributed to the disordering of an unspecified long-range order within noncrystalline domains[28,30,31] and to the order–disorder transition, otherwise called the microphase-separation transition.[26,27,35–37] A decrease in the scattering intensity has been observed to coincide with this endotherm in small-angle X-ray scattering/DSC studies,[26,35,37] providing strong evidence to support the latter explanation. This endotherm is attributed here to the disordering of the hard microdomains. Segmental mixing had already taken place in the 476 materials at the T_1 endotherm. The increase in the temperature of hard-segment disordering between the 793 and 998 materials can be attributed to the average length of the hard segments increasing with the soft-segment length. The enthalpy associated with the bimodal T_2 endotherm was not significantly different between the two polymers. The 998 material did not display the T_3 endotherm associated with the melting of the crystalline hard-segment material reported by Martin et al.[13,14] because the hard segments were incapable of crystallizing at the low temperatures involved with the solution-casting (60°C) and annealing (80°C) process employed here.

Dynamic mechanical properties

The dissipation factor (tan δ) and storage modulus (E') are given as functions of temperature in Figures 5 and 6, respectively. Two loss peaks were observed for all materials, and the peak temperatures are provided in Table IV. The secondary loss peak at approximately −90°C is designated the γ peak.[38] The γ relaxation is tentatively assigned to a crankshaft-like motion of methylene sequences, and the main contribution is expected to arise from the methylene sequences in the soft segment, as opposed to the butanediol chain extender.[38] An increase in the soft-segment length and hence microphase separation resulted in a decrease in the γ-relaxation temperature. The temperature and intensity of the γ loss peak were not affected by the addition of layered silicates.

The primary loss peak coincided with a reduction in E' of approximately 2 orders of magnitude and was assigned to the glass transition of the soft-segment-

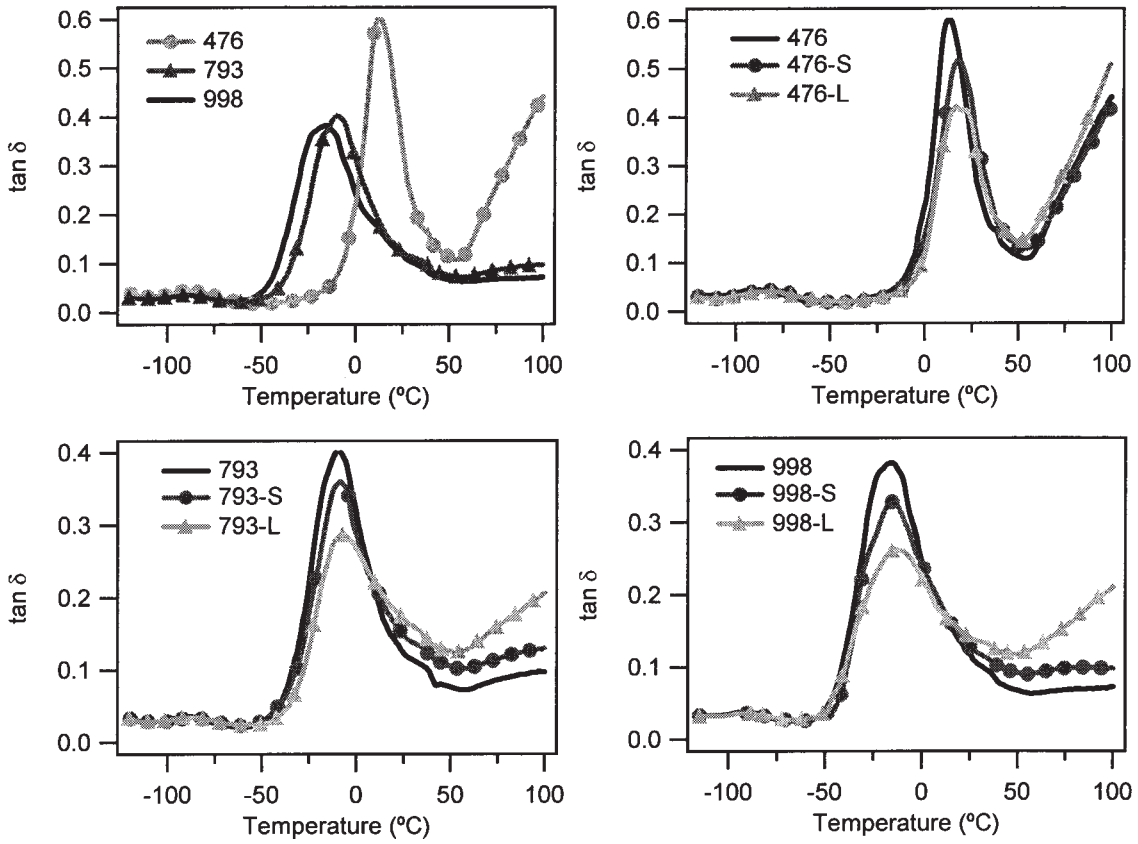

Figure 5 Tan δ as a function of temperature.

rich phase.[38] An increase in the soft-segment molecular weight led to a decrease in T_g, a reduction in the intensity of the loss peak, and a broadening of the temperature range over which T_g occurred. T_g decreased with an increase in the soft-segment molecular weight because of the increased phase separation. The T_g range became broader with an increase in the soft-segment molecular weight because of the greater range of molecular environments experienced by the soft segments. As the phase separation increased, a percentage of the soft segments became further removed from the hard segments, and this lowered the onset temperature of the transition. At the same time, the presence of longer hard segments and purer hard domains resulted in greater soft-segment motion restrictions in the interfacial region and in the soft phase in which dissolved hard segments resided, causing a broadening of T_g.

The addition of layered silicates caused an increase in E' over the entire temperature range. The increase in E' on filler addition was more significant above T_g because of the greater mismatch in the elastic constants of the polymer and filler.[39] The addition of layered silicates caused a slight increase in T_g and a reduction in the damping capacity. This was attributed to the layered silicates restricting molecular motion. The L silicate resulted in a larger increase in E' and T_g because the amount of the polymer restrained by the silicates increased with the particle diameter.[17] Tan δ is equal to E''/E', where E'' is the loss modulus. The reduction in the intensity of the tan δ peak was caused by an increase in E' (Fig. 6). Although the addition of fillers also caused an increase in E'' (data not shown), this increase was not as significant as that of E' at T_g.

The intensity of the tan δ curve increased sharply with temperatures above 50°C for the pure 476 polymer. This coincided with the onset of complete segmental mixing resulting from the disordering of the single MDI sequence structures, as observed via DSC. This feature was less prominent for the 793 and 998 host polymers because their hard domains remained intact in this temperature range.

The addition of layered silicates also brought about an increase in the intensity of the tan δ curve above 50°C in the 793 and 998 host polymers. Although this feature was similar to that displayed by the 476 host polymer, the mechanism responsible for this behavior was different. Layered silicates are known to cause an increase in the damping capacity between T_g and the melting point of the host polymer because of their greater influence on E'' with respect to E' in this temperature range.[17]

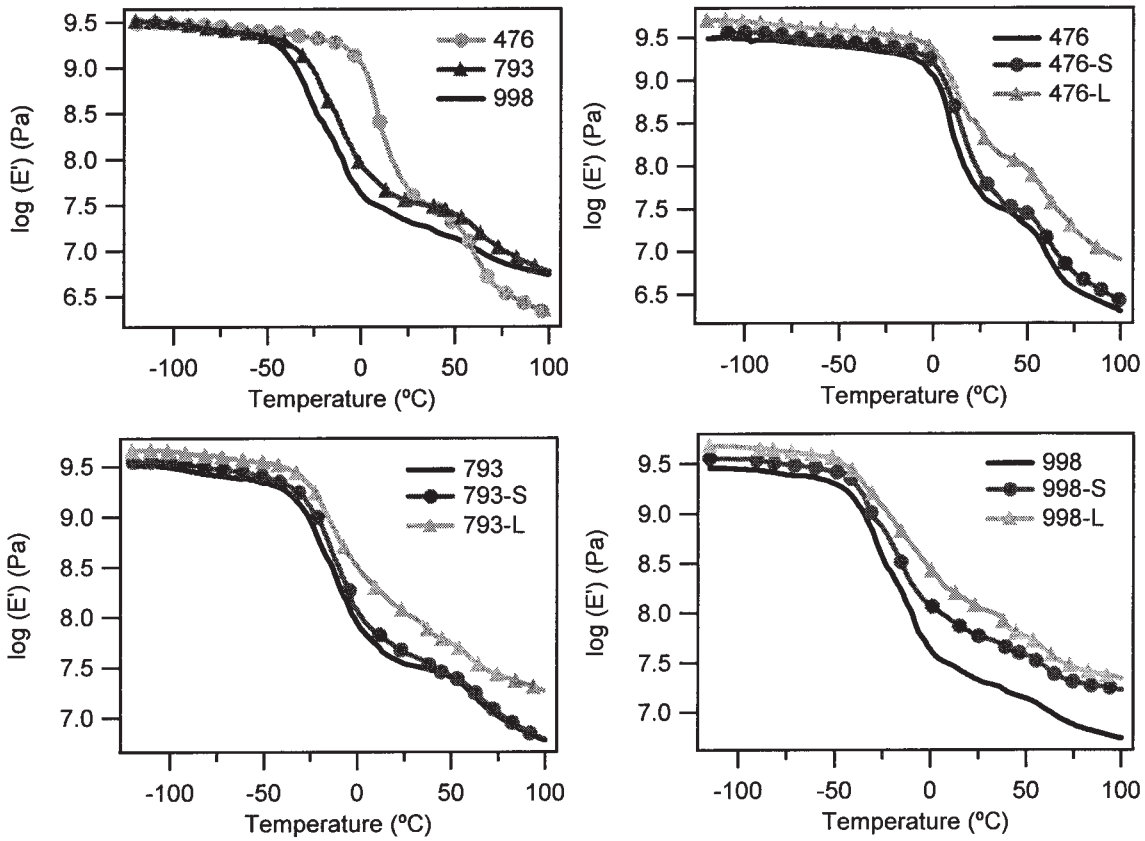

Figure 6 E' as a function of temperature.

Mechanical properties

Stress–strain curves of the composites are shown in Figure 7. Young's modulus was calculated as the slope at 0% strain, and the values are given in Table V. Martin et al.[13] reported an increase in stiffness as the block length and degree of phase separation increased in these TPUs when they were compression-molded. This trend was not observed with solvent processing. The modulus became greater as the soft-segment length and phase separation increased from 476 to 793 g/mol. However, the modulus decreased for 998, which was the most phase-separated TPU and furthest above its T_g. This was because the melt-processing-induced hard-segment crystallization that previously caused a significant stiffening and reinforcement of the soft phase of 998 was absent.[13]

TABLE IV
DMTA Loss Peaks

	Relaxation	
	γ (°C)	T_g (°C)
476	−83	13
476-S	−82	18
476-L	−83	19
793	−89	−9
793-S	−87	−8
793-L	−88	−7
998	−91	−16
998-S	−90	−15
998-L	−90	−13

The addition of layered silicates resulted in an increase in Young's modulus. The mechanical restraint experienced by the polymers increased with the particle size, and the increase in stiffness caused by the L silicate was observed over the entire stress–strain curve. The percentage increase in the modulus of the L composites became greater as the soft-segment length and phase separation of the host TPU decreased. This was presumably the result of an increase in the proportion of urethane linkages available to form secondary bonds with the MEE surface as the soft-segment length and phase separation decreased; this resulted in the formation of a more rigid intercalated structure. The higher increase in the modulus with decreasing TPU segment length is not believed to be a result of increased filler dispersion because particle thickness calculations from the XRD data implied that the aspect ratio and the degree of delamination of the L silicate increased with the soft-segment length.

The ultimate tensile properties of the pure polymers were significantly higher when they were prepared by

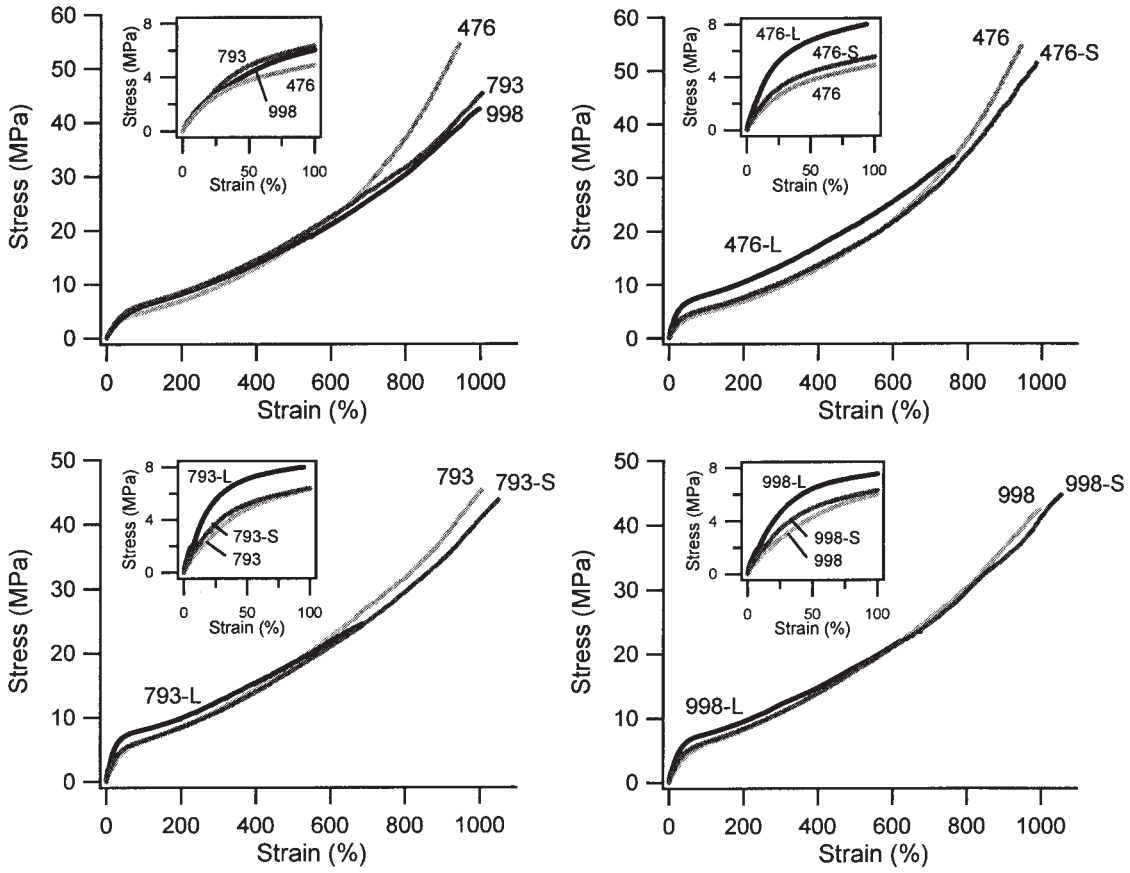

Figure 7 Stress–strain behavior.

solvent casting instead of compression molding[13] because significant thermal degradation occurs during the melt processing of TPUs.[40,41] The high ultimate tensile properties of the solvent-cast 793 and 998 polymers could also be attributed to the absence of melt-processing-induced hard-segment crystallization,[13] would could cause a significant stiffening of the TPU and a reduction in the chain mobility and ultimate tensile properties. The pure 793 and 998 host polymers exhibited almost identical stress–strain curves. 476 was approximately 10 MPa stronger than the other host polymers and displayed a sharper upturn in the stress–strain curve. This indicated that the short-segment TPU was capable of stronger secondary bonding at a high strain, presumably because of the increased number of urethane linkages available due to the phase-mixed morphology and the greater number of hard segments in 476.

TABLE V
Modulus Values Obtained from the Stress–Strain Data

	Young's modulus (MPa)	Increase in young's modulus (%)
476	12.8	—
476-S	16.4	30
476-L	27.1	110
793	14.8	—
793-S	18.6	30
793-L	26.2	80
998	12.8	—
998-S	16.2	30
998-L	21.4	70

The addition of the L silicate caused a significant reduction in the ultimate tensile properties of the three TPUs because of the high mechanical restraint imparted by the large diameter particles. Void formation at the sites of the large tactoids is thought to have contributed to the poor ultimate tensile properties of these composites.[12,42] The S silicate did not have a discernible effect on the overall stress–strain response of the three PHMO TPUs. This is in contrast to the enhancement of the tensile strength and upturn in the stress–strain curve achieved when the S silicate was incorporated into a TPU with a PTMO soft segment (Fig. 8), particularly at a lower filler concentration, as described elsewhere.[12] This result indicates that the interaction between the soft segment and the MEE surface is critical to increasing the tensile strength via an upturn in the stress–strain curve. PTMO is a more hydrophilic and mobile soft segment than PHMO be-

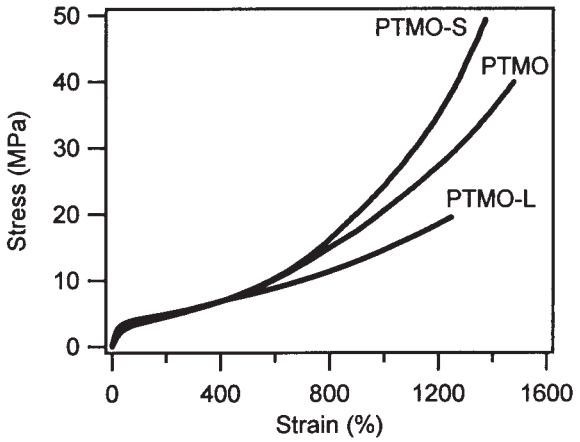

Figure 8 Stress–strain behavior of the PTMO-soft-segment TPU nanocomposites.

cause of the lower number of methylene sequences between ether oxygens in the backbone. As a result, the PTMO soft segment enables greater secondary bonding to occur between the TPU and the organosilicate surface, resulting in improved stress transfer to the filler and reduced molecular slippage.

In addition to factors such as the filler type, concentration, dispersion, aspect ratio, orientation, and polymer–filler interaction, the importance of the host polymer molecular weight for the composite properties has been reported.[43,44] The PTMO-based TPU has a higher molecular weight than the PHMO-based TPUs. At this stage, it is not known to what extent, if any, the higher molecular weight of the PTMO-based TPU contributed to the tensile property improvements observed for this nanocomposite system.

CONCLUSIONS

Two organically modified layered silicates (with small and large particle diameters) were incorporated into three segmented polyurethanes with various degrees of microphase separation. The extent of microphase separation was increased by an increase in the molecular weight of the PHMO soft segment. The interlayer spacing measured via XRD indicated that the molecular weight of the soft segment did not influence the amount of polyurethane intercalating the interlayer spacing within the range under investigation (476–998 g/mol). The average particle thickness estimated from XRD data indicated that the particles became thinner with increasing soft-segment molecular weight, probably because of viscosity differences between the host polymers during the high shear mixing step of solution processing. The addition of layered silicates did not affect the bulk microphase morphology of the three host polymers, regardless of the nanofiller size.

The addition of the layered silicates resulted in an increase in stiffness, particularly in the case of the large size fraction, because the mechanical restraint of the TPU chains increased with the layered silicate size. The stiffness enhancement increased as the segment length and microphase separation of the polyurethane decreased, presumably because a higher concentration of urethane linkages were available to interact with the filler.

The ultimate tensile properties of the PHMO host polymers were significantly higher when they were solution-processed instead of being melt-processed.[13] The negative impact of melt processing on the mechanical properties was attributed not only to thermal degradation but also to hard-segment crystallization, which reduced chain mobility and secondary bonding at high elongation. The incorporation of the large silicate caused a reduction in the ultimate tensile properties because of the high mechanical restraint imparted to the TPUs. The ultimate tensile properties of the PHMO TPUs were not affected by the addition of the small silicate. This is in contrast to the enhancement in the tensile strength and the upturn in the tensile curve observed when the small silicate was incorporated into a TPU with a PTMO soft segment.[12] It is proposed that the polyurethane nanocomposite containing the more hydrophilic and mobile PTMO soft segment is capable of greater secondary bonding between the polyurethane chains and the organosilicate surface, resulting in improved stress transfer to the filler and reduced molecular slippage.

The authors thank Jeremy Ruggles and Ian Gentle for useful discussions and Stephen King, Philip Reynolds, and Adam Perriman for their assistance in running the small-angle neutron scattering experiments.

References

1. Ray, S. S.; Okamoto, M. Prog Polym Sci 2003, 28, 1539.
2. Alexandre, M.; Dubois, P. Mater Sci Eng 2000, 28, 1.
3. Giannelis, E. P. Adv Mater 1996, 8, 29.
4. Kojima, Y.; Usuki, A.; Kawasumi, M.; Okada, A.; Fukushima, Y.; Kurauchi, T.; Kamigaito, O. J Mater Res 1993, 8, 1185.
5. Hasegawa, N.; Usuki, A. Polym Bull 2003, 51, 77.
6. Yurekli, K.; Karim, A.; Amis, E. J.; Krishnamoorti, R. Macromolecules 2003, 36, 7256.
7. Silva, A. S.; Mitchell, C. A.; Tse, M. F.; Wang, H. C.; Krishnamoorti, R. J Chem Phys 2001, 115, 7166.
8. Krishnamoorti, R.; Silva, A. S.; Mitchell, C. A. J Chem Phys 2001, 115, 7175.
9. Wang, K. H.; Choi, M. H.; Koo, C. M.; Xu, M. Z.; Chung, I. J.; Jang, M. C.; Choi, S. W.; Song, H. H. J Polym Sci Part B: Polym Phys 2002, 40, 1454.
10. Wang, K. H.; Xu, M.; Choi, T. K.; Chung, I. J. Polym Bull 2001, 46, 499.
11. Maiti, P.; Yamada, K.; Okamoto, M.; Ueda, K.; Okamoto, K. Chem Mater 2002, 14, 4654.
12. Finnigan, B.; Jack, K.; Campbell, K.; Halley, P.; Truss, R.; Casey, P.; Cookson, D.; King, S.; Martin, D. Macromolecules 2005, 38, 7386.

13. Martin, D. J.; Meijs, G. F.; Renwick, G. M.; McCarthy, S. J.; Gunatillake, P. A. J Appl Polym Sci 1996, 62, 1377.
14. Martin, D. J.; Meijs, G. F.; Gunatillake, P. A.; McCarthy, S. J.; Renwick, G. M. J Appl Polym Sci 1997, 64, 803.
15. Yang, J. H.; Han, Y. S.; Choy, J. H.; Tateyama, H. J Mater Chem 2001, 11, 1305.
16. Campbell, K. Ph.D. Thesis, University of Queensland, 2005.
17. Fornes, T. D.; Paul, D. R. Polymer 2003, 44, 4993.
18. Koberstein, J. T.; Stein, R. S. J Polym Sci Polym Phys Ed 1983, 21, 2181.
19. Wignall, G. D.; Bates, F. S. J Appl Crystallogr 1987, 20, 28.
20. Vaia, R. A.; Liu, W. D. J Polym Sci Part B: Polym Phys 2002, 40, 1590.
21. Laity, P. R.; Taylor, J. E.; Wong, S. S.; Khunkamchoo, P.; Norris, K.; Cable, M.; Andrews, G. T.; Johnson, A. F.; Cameron, R. E. Polymer 2004, 45, 7273.
22. Martin, D. J.; Meijs, G. F.; Gunatillake, P. A.; Yozghatlian, S. P.; Renwick, G. M. J Appl Polym Sci 1999, 71, 937.
23. Krakovsky, I.; Bubenikova, Z.; Urakawa, H.; Kajiwara, K. Polymer 1997, 38, 3637.
24. Vaia, R. A.; Liu, W. D.; Koerner, H. J Polym Sci Part B: Polym Phys 2003, 41, 3214.
25. Reynolds, P. A.; Gilbert, E. P.; White, J. W. J Phys Chem B 2000, 104, 7012.
26. Koberstein, J. T.; Russell, T. P. Macromolecules 1986, 19, 714.
27. Saiani, A.; Daunch, W. A.; Verbeke, H.; Leenslag, J. W.; Higgins, J. S. Macromolecules 2001, 34, 9059.
28. Seymour, R. W.; Cooper, S. L. Macromolecules 1973, 6, 48.
29. Chen, T. K.; Shieh, T. S.; Chui, J. Y. Macromolecules 1998, 31, 1312.
30. Vanbogart, J. W. C.; Bluemke, D. A.; Cooper, S. L. Polymer 1981, 22, 1428.
31. Hesketh, T. R.; Vanbogart, J. W. C.; Cooper, S. L. Polym Eng Sci 1980, 20, 190.
32. Koberstein, J. T.; Galambos, A. F.; Leung, L. M. Macromolecules 1992, 25, 6195.
33. Hu, W. C.; Koberstein, J. T. J Polym Sci Part B: Polym Phys 1994, 32, 437.
34. Koberstein, J. T.; Stein, R. S. J Polym Sci Polym Phys Ed 1983, 21, 1439.
35. Ryan, A. J.; Macosko, C. W.; Bras, W. Macromolecules 1992, 25, 6277.
36. Leung, L. M.; Koberstein, J. T. Macromolecules 1986, 19, 706.
37. Li, Y. J.; Gao, T.; Liu, J.; Linliu, K.; Desper, C. R.; Chu, B. Macromolecules 1992, 25, 7365.
38. Huh, D. S.; Cooper, S. L. Polym Eng Sci 1971, 11, 369.
39. Buxton, G. A.; Balazs, A. C. J Chem Phys 2002, 117, 7649.
40. Finnigan, B.; Martin, D.; Halley, P.; Truss, R.; Campbell, K. Polymer 2004, 37, 2149.
41. Finnigan, B.; Martin, D.; Halley, P.; Truss, R.; Campbell, K. J Appl Polym Sci 2005, 97, 300.
42. Kim, G. M.; Lee, D. H.; Hoffmann, B.; Kressler, J.; Stoppelmann, G. Polymer 2001, 42, 1095.
43. Sternstein, S. S.; Zhu, A. J. Macromolecules 2002, 35, 7262.
44. Fornes, T. D.; Yoon, P. J.; Keskkula, H.; Paul, D. R. Polymer 2001, 42, 9929.